Supporting Information

Nanoconfined growth of lithium-peroxide inside electrode pores: A noncatalytic strategy toward mitigating capacity-rechargeability trade-off in Lithium–Air battery

Arghya Dutta*, Kimihiko Ito and Yoshimi Kubo*

1. Experimental section

1.1. Synthesis of mesoporous carbons

Mesoporous carbons were synthesized by a hard-templating pathway where mesoporous SBA-15 silica was used as the hard template while phenol-formaldehyde mixture with or without urea was chosen to be the carbon precursor.

1.1.1. Synthesis of SBA-15: Mesoporous SBA-15 silica was synthesized by a soft templating procedure using tetraethyl orthosilicate (TEOS, Wako) as the silica source and triblock co-polymer poly(ethylene oxide)–poly(propylene oxide)–poly(ethylene oxide) (PEO–PPO–PEO, Pluronic® P123, Sigma Aldrich, M_n ~5800) as the soft template. At first, the triblock co-polymer template (1.0 g) was dissolved in 2.0 M hydrochloric acid (30 mL HCl, Wako Pure Chemicals, 35–37%) and TEOS (2.1 g) was slowly added. The reaction mixture was continued to stir at 40 ℃ inside a polypropylene bottle for 24 h. After that, the polypropylene bottle was kept at 100 ℃ for another 24 h for hydrothermal reaction. The resulting solid SBA-15 silica was filtered, washed thoroughly with Milli-Q® H_2O and dried at 70 ℃. Finally, the organic template was removed by calcination of the as-prepared nanostructured SBA-15 in air at 600 ℃ for 5 h.

1.1.2. Synthesis of CMK-3: Mesoporous CMK-3 was synthesized by following a previously reported procedure.[1] Briefly, phenol (0.6 g (0.0064 mol), Wako Pure Chemicals, 99%) and formaldehyde (1.0 g (~ 0.012 mol), Wako Pure Chemicals, 36–38%) were dissolved in Milli-Q® H_2O (6 mL) and to this solution mesoporous SBA-15 (0.5 g) was added. The mixture was stirred at 25 ℃ for 1 h, small amount of concentrated H_2SO_4 (100 µL) was very slowly added, the temperature was increased up to 80 ℃ and the stirring was continued until the mixture became dry. The dry reaction mixture was heated at 150 ℃ for 3 h and the carbon precursor impregnation steps were repeated with half the amounts of phenol (0.3 g) and formaldehyde (0.5 g) used in the previous step. Carbonization of the sample was carried out by pyrolysis of the composite at 950 ℃ for 6 h under flowing Ar. Finally, SBA-15 template was etched by stirring the sample in 10% aqueous hydrofluoric acid (10 mL, HF, Wako Pure Chemicals, 46–

48%) for 10 h and the etching process was repeated once. The silica-free mesoporous CMK-3 was collected by centrifugation after washing with Milli-Q® H_2O for several times until no acid in the washing liquid was noticed by pH paper and the carbon was dried at 110 ℃ for 12 h under vacuum.

1.1.3. Synthesis of N-doped CMK-3: N-doping of CMK-3 was carried out by using urea as the nitrogen precursor added to phenol-formaldehyde mixture. The amount of formaldehyde was kept constant while the ratio of phenol and urea was varied in such a way that roughly maintained the formaldehyde to urea + phenol mole ratio of 2:1. In a typical synthesis, formaldehyde (1.0 g, ~ 0.012 mol) was dissolved in Milli-Q® H_2O (6 mL) and the pH of the solution was adjusted to ~ 8 by using 2 N NaOH. Four different mixtures of urea and phenol in the ratios (*mol*/*mol*) (1:2.5, 1:1.5, 1:1 and 1:0.6) were added to the formaldehyde solution while stirring. After complete dissolution of all the reagents, SBA-15 template (0.5 g) was added, stirred at 25 ℃ for 30 min and then while stirring the temperature was increased up to 80 ℃ until the reaction mixture became dry. The dry solid was kept at 150 ℃ for 5 h and the precursor impregnation was repeated with half the amounts of reagents previously used. The carbonization and template removal steps were same as described for CMK-3. The N-doped samples were labeled as NCMK-3-1 to -4 in the increasing order of fraction of urea used during synthesis.

1.2. Electrode fabrication

In addition to mesoporous carbons, multiwalled carbon nanotubes (CNT, TCI Chemicals, average outer diameter of 20-40 nm and length of 5-15 μm), Super P carbon particles (SP, Alfa Aesar, ~ 50-70 nm diameter) and Ketjenblack particles (KB, EC600JD, Lion, ~ 40-60 nm diameter) were also used as electrode materials for comparison. Slurries of different carbons were prepared by using LITHion™ (Ion Power) as the binder (4:1 ratio (*w*/*w*) for carbon/LITHion) and N-methyl-2-pyrrolidone (NMP) as the solvent. The slurries were tape casted on carbon paper (CP, TGP-H-30, Toray), dried slowly at room temperature followed by vacuum drying at 110 ℃ for 12 h, and finally cut into 1.6 cm diameter electrode (~ 2 cm^2 geometric area). The average carbon loading for all the electrodes was ~ 0.5 mg cm^{-2}.

1.3. Li–O_2 cell assembly and testing

All the Li–O_2 cells were assembled and tested inside a dry-room (dew point of < –60 ℃) without exposing to ambient conditions. Coin type CR2032 cells with perforated stainless-steel cases (Hohsen Corp.) were assembled inside an isolated draft chamber under flowing oxygen with

dew point of < –90 ℃ (< 0.1 ppm H_2O). A typical Li–O_2 cell is composed of a Li metal (1.6 cm in diameter, 200 μm thickness, Honjo Metal) negative electrode, two separators of Celgard® 2325 (1.6 cm in diameter) and glass fiber (GF/C, 1.6 cm in diameter, Whatman®) and the positive electrode of different carbon materials. 1 M Lithium bis(trifluoromethanesulfonyl)imide (LiTFSI, Kishida Chemical Co., Ltd.) dissolved in anhydrous (< 20 ppm H_2O measured by Karl Fisher titration) tetraethylene glycol dimethyl ether (TEGDME, Japan Advanced Chemicals) was used as the electrolyte in most of the experiments unless otherwise mentioned. 1 M lithium nitrate ($LiNO_3$, Sigma Aldrich) as the electrolyte salt and 0.05 M 2,5-di-tert-butyl-1,4-benzoquinone (DBBQ, Sigma Aldrich) as the electrolyte additive were also used as specifically mentioned. The Li–O_2 coin cells were tested under either flowing oxygen (dew point of < –90 ^oC (< 0.1 ppm H_2O)) or dry air (dew point of < –60 ^oC (< 11 ppm H_2O)) using a galvanostatic electrochemical tester (HJ1001SD8, Hokuto Denko) at ~ 25 ^oC. Cyclic voltammetry (CV) experiments of symmetric Carbon|separator|Carbon coin cells to measure electrochemically active surface area (ECSA) were tested on an Autolab PGSTAT128N in the range 0 to 1 V at a sweep rate of 50 mV s^{-1}. CV measurements under 3-electrode set up were carried out using Autolab PGSTAT128N and a Pine Modulated Speed Rotator (MSR) fitted with rotating disk electrode (RDE) where different carbons were used as the disk, while metallic lithium served as both counter and reference electrodes in 1 M LiTFSI/TEGDME electrolyte. Carbon slurries, similar to mentioned above, were drop-casted on a GC disk (0.25 cm^2) to prepare the electrode. The sweep rates were 0.5 and 0.05 mV s^{-1} for ORR and OER respectively without rotation of the electrode. Oxygen gas was bubbled through the electrolyte for 1 h before starting CV measurements to ensure saturation and oxygen was continued to flow through the vessel at the time of measurement. Electrochemical impedance spectra were measured using Biologic VSP potentiostat/galvanostat while a current was drawn (GEIS) in the frequency range 200 kHz to 1 mHz. Impedance of the cells with KB and N-CMK-3-3 electrodes were measured under open circuit potential at 1 h interval during discharge at 100 mA g^{-1} in dry air. The alternating current (AC) amplitude for GEIS measurement was set at 10 μA.

1.4. Characterization

After discharge of the cells, positive electrodes were taken out, rinsed with dehydrated tetrahydrofuran (< 10 ppm H_2O, Wako), dried under vacuum and used for post-mortem analyses. To avoid exposure of the samples to ambient atmosphere during characterization, hermetic transfer vessels were used in all cases. Powder X-ray diffraction (XRD) patterns of

the as-prepared and discharged electrodes were measured on a D8 ADVANCE (Bruker) diffractometer with a CuKα source (λ CuKα = 1.542 Å). Fourier transform infrared (FTIR) spectra were obtained using Nicolet iS50 (Thermo Fisher Scientific) in Attenuated total reflection (ATR) mode with DLaTGS-CsI detector and CsI beamsplitter. X-ray photoelectron spectra (XPS) were collected on a VersaProbe II Scanning XPS Microprobe (ULVAC-PHY). Morphologies of the as-prepared carbons and discharge products were observed on a JSM-7800F field-emission scanning electron microscope (FE-SEM, JEOL) with 5 keV accelerating voltage and chemical composition of the carbon materials were analyzed on an energy dispersive X-ray spectrometer (X-Max^N 50, Oxford) fitted with the SEM. The pore structures of the mesoporous carbons were observed on a JEOL JEM-ARM200F (accelerating voltage 200 kV) transmission electron microscope (TEM). Viscosity of the electrolyte was measured by using a rolling-ball viscometer (Lovis 2000 ME, Anton Paar). UV-vis spectra for the titration of discharged Li_2O_2 were collected on a Shimadzu UV 2600 spectrophotometer. The discharged electrodes along with separators were soaked in $TiOSO_4$ solution (3 mL) (1.9-2.1%, Sigma Aldrich) + Milli-Q® H_2O (10 mL) for 1 h and the absorbances of the solutions were measured at the wavelength 407 nm. Quantification of Li_2O_2 in the electrodes were done by correlating the measured absorbance with a calibration curve reported previously.[2] Online electrochemical mass spectrometry (OEMS) measurements during recharge of the cells were carried out in a home-made system using a quadrupole mass spectrometer (JMS-Q1500, JEOL). The flow-type electrochemical cells for OEMS were assembled using the same components (Li|separator|carbon) as described above. The evolved gases during charging were continuously measured by flowing He as the carrier gas at a rate of 2 mL min^{-1}.

2. Determination of the hydrodynamic radii of the electroactive species in the electrolyte

Hydrodynamic radii of the electroactive species were determined by the Stokes-Einstein equation

$$D = \frac{k_B T}{6\pi\mu r} \quad (1)$$

where D, k_B, T, μ and r are the diffusion coefficient of the electroactive species, Boltzmann constant, temperature, viscosity of the electrolyte and hydrodynamic radius of the electroactive species in the electrolyte solution, respectively.

k_B (m^2 kg s^{-2} K^{-1})	T (K)	μ (mPa s)	D_{O_2} (m^2 s^{-1})	r_{O_2} (nm)	D_{Li^+} (m^2 s^{-1})	r_{Li^+} (nm)	D_{TFSI^-} (m^2 s^{-1})	r_{TFSI^-} (nm)
1.38×10^{-23}	298	11.57	1.6×10^{-11}[a]	1.18	4.6×10^{-11}[b]	0.41	6.7×10^{-11}[c]	0.28

[a]From Gittleson *et al*.[3]

[b, c]Calculated by extrapolating the data set from Saito *et al*. up to 298 K.[4]

3. Electrochemically active surface area (ECSA) measurement

ECSA of all the carbon electrodes was measured by following a previously reported procedure.[2] Cyclic voltammetry (CV) of symmetric Carbon|separator|Carbon coin type 2032 cells with 100 µL 1 M LiTFSI/TEGDME electrolyte (< 20 ppm H_2O) was carried out in the range 0 to 1 V at a sweep rate of 50 mV s^{-1}. From the CV result, at first, the capacitance of a carbon electrode was calculated by using the equation

$$C = \int_{E_1}^{E_2} \frac{i\,(E)dE}{2(E_2 - E_1)mv}$$

where C is the specific capacitance of a single electrode. E_1, E_2 are the lower and upper limits of cut-off potentials for CV respectively, i (E) is the instantaneous current, m is the mass of a single electrode and v is the scan rate of CV. The capacitance was calculated from 400th cycle of CV.

After obtaining the specific capacitance, ECSA of an electrode was calculated from:

$$C = \frac{\varepsilon\,\varepsilon_0 A}{d}$$

where ε is the relative dielectric constant of teraglyme (7.79), ε_0 is the permittivity of vacuum (8.85×10^{-12} F m^{-1}), A is the ECSA and d is the electric double layer thickness assumed to be the radius of oxygen molecules (~1.5 Å).

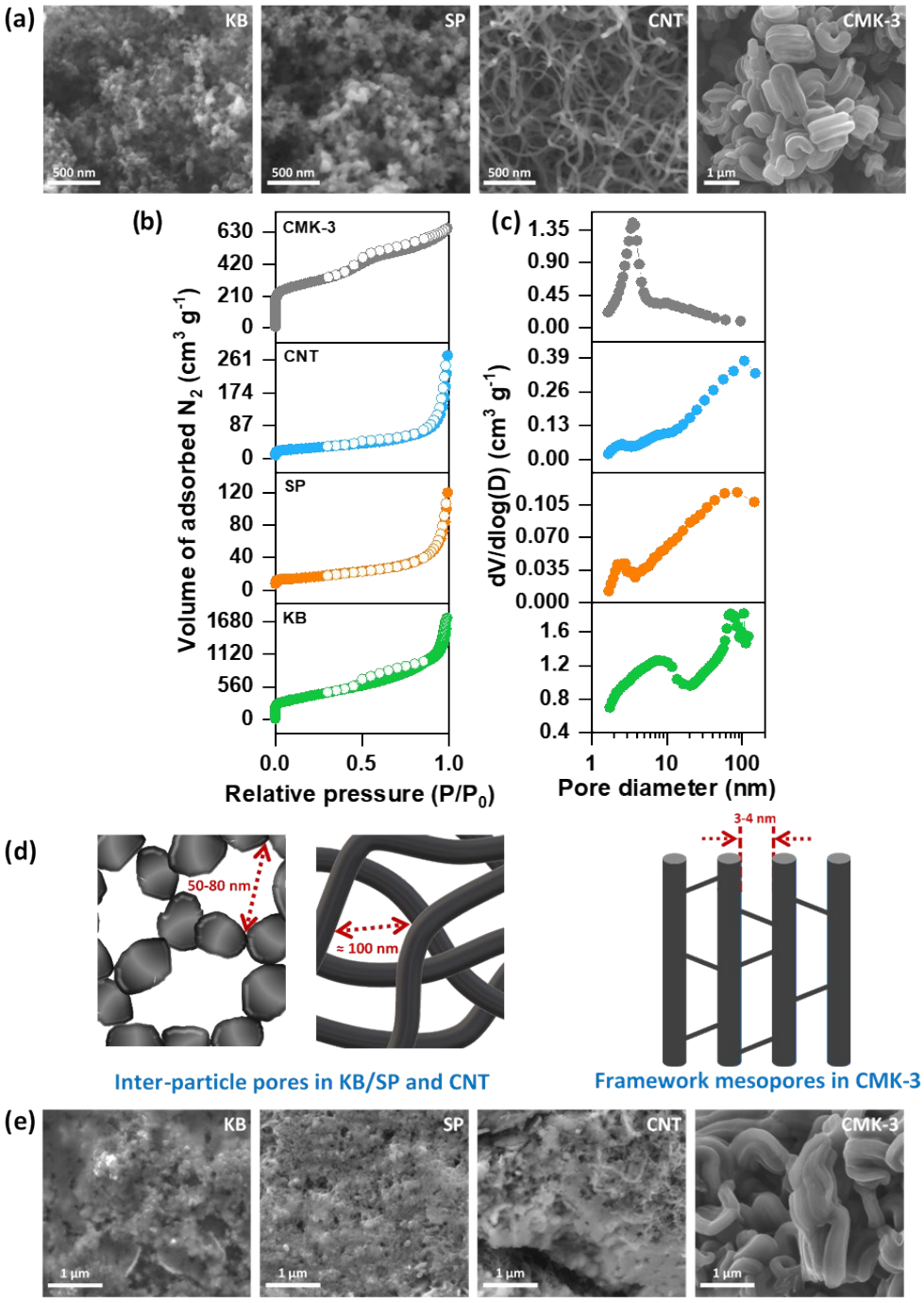

Figure S1. (a) Scanning electron microscopy (SEM) images of as received/prepared KB, SP, CNT and CMK-3 carbons. (b) Nitrogen adsorption/desorption isotherms of different carbons measured at –196 ℃ and (c) pore-size analysis by Barrett-Joyner-Halenda (BJH) method. (d) schematic illustration of pore structure in these four carbons. (e) SEM images of KB, SP, CNT and CMK-3 electrodes after discharge up to 2 V *vs.* Li/Li^+ in 1 M LiTFSI/tetraglyme electrolyte at 100 mA g^{-1} under dry air.

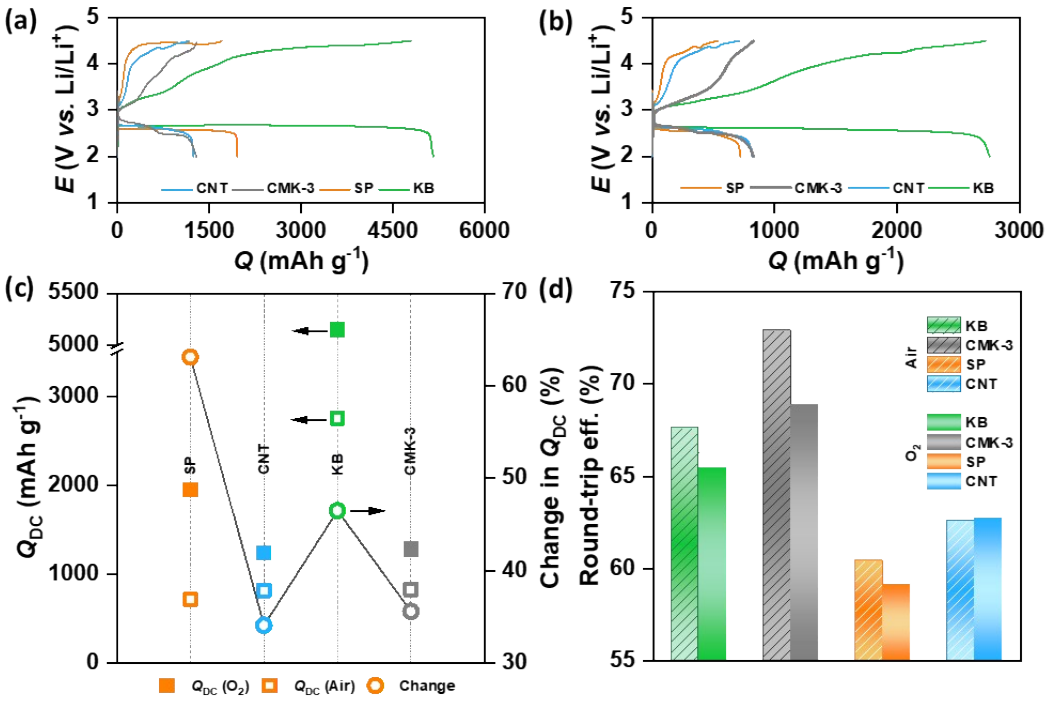

Figure S2. Galvanostatic DC/RC profiles of (a) Li–O_2 and (b) Li–Air cells with different electrodes in 1 M LiTFSI/tetraglyme electrolyte in the potential range 2–4.5 V *vs*. Li/Li^+ at the same current density of 100 mA g^{-1}, (c) Comparison of discharge capacities of the electrodes in pure oxygen and dry air and (d) Comparison of round-trip efficiencies of the electrodes in both Li–O_2 and Li–Air cells.

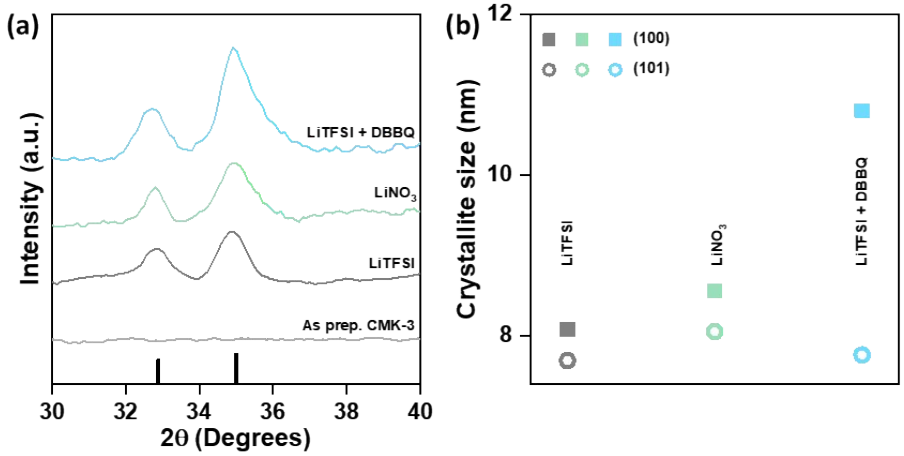

Figure S3. (a) X-ray diffraction (XRD) patterns of the CMK-3 electrodes discharged in different electrolytes and additives up to 2 V *vs*. Li/Li^+ at the same current density of 100 mA g^{-1} under dry air along with XRD peak positions for standard Li_2O_2 sample shown by black vertical lines at the bottom and (b) Comparison of lithium-peroxide (Li_2O_2) crystallite size deposited in different electrolytes.

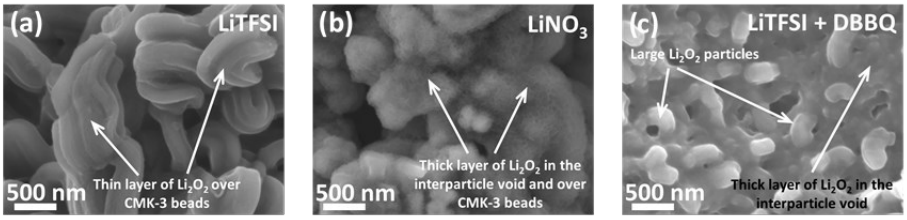

Figure S4. Scanning electron microscopy (SEM) images of CMK-3 electrodes after DC in (a) 1 M LiTFSI/tetraglyme, (b) 1 M $LiNO_3$/tetraglyme and (c) 1 M LiTFSI + 0.05 M DBBQ/tetraglyme electrolytes.

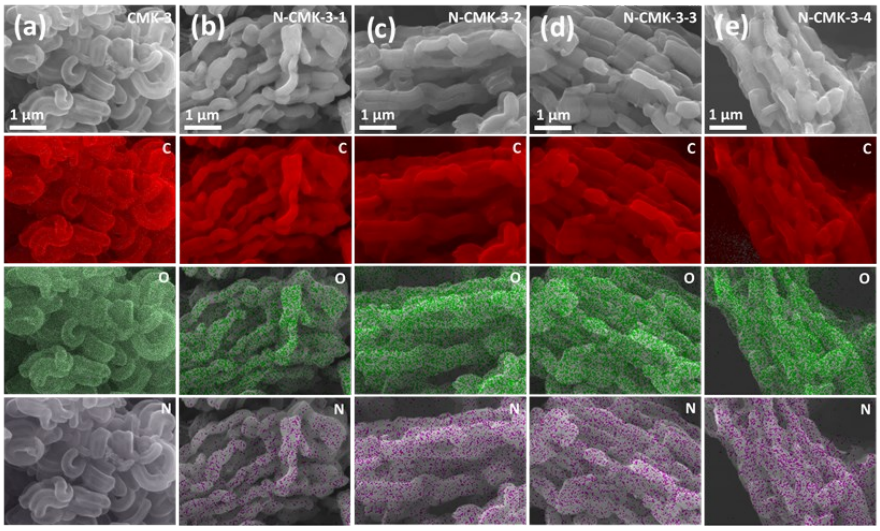

Figure S5. SEM images of as-prepared (a) CMK-3, (b) N-CMK-3-1, (c) N-CMK-3-2, (d) N-CMK-3-3 and (e) N-CMK-3-4 carbons with corresponding energy dispersive X-ray (EDX) mapping for carbon, oxygen and nitrogen.

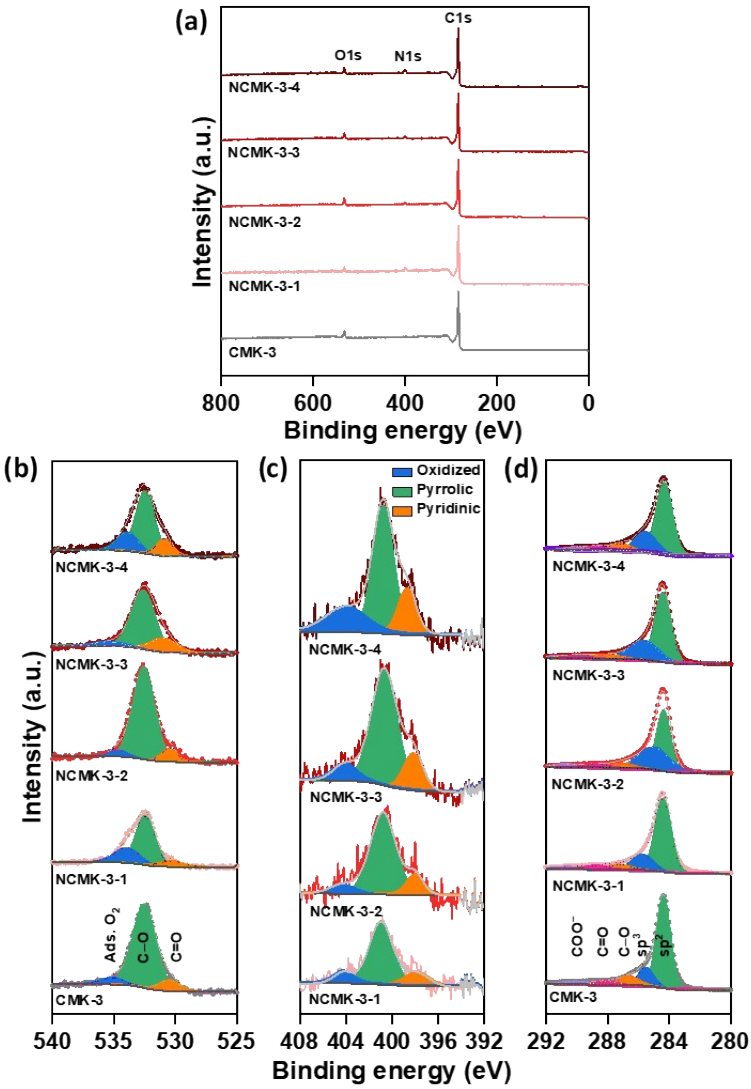

Figure S6. (a) Wide-scan, (b) O1s, (c) N1s and (d) C1s X-ray photoelectron spectra (XPS) of CMK-3 and N-CMK-3 carbons.

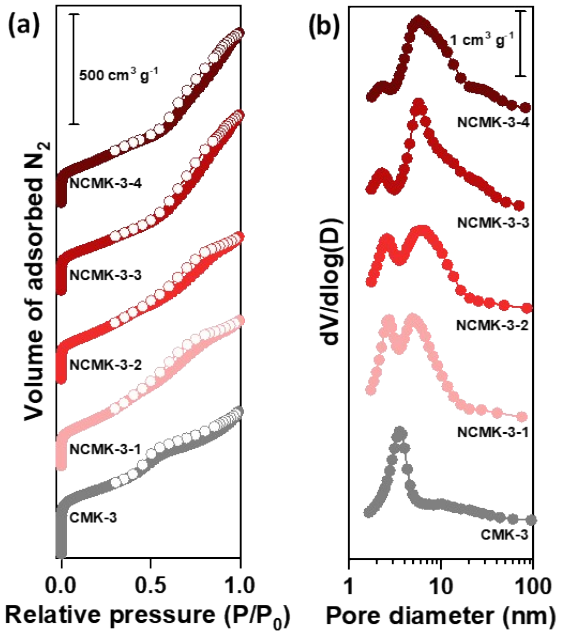

Figure S7. (a) Nitrogen adsorption/desorption isotherms of different mesoporous carbons measured at –196 ℃ and (b) pore-size analysis by Barrett-Joyner-Halenda (BJH) method.

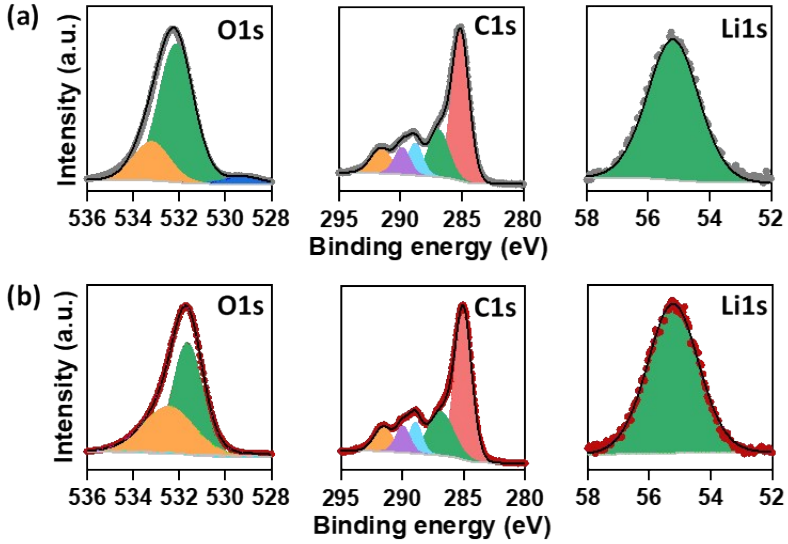

Figure S8. O1s, C1s and Li1s XPS of (a) CMK-3 and (b) N-CMK-3-3 electrodes discharged in 1 M LiTFSI/tetraglyme electrolyte under dry air.

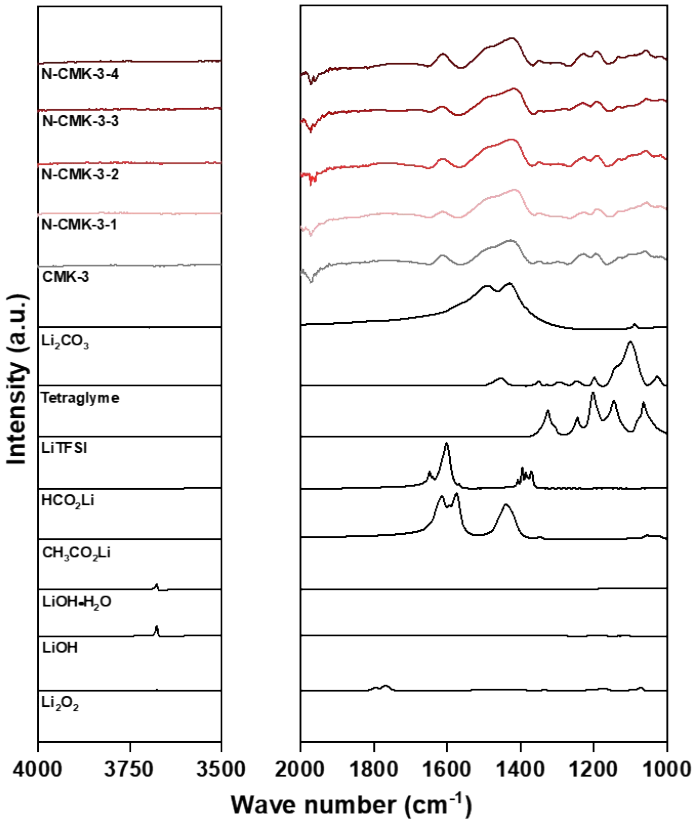

Figure S9. Fourier transform infrared (FTIR) spectra of CMK-3 and N-CMK-3 electrodes discharged in 1 M LiTFSI/tetraglyme under dry air.

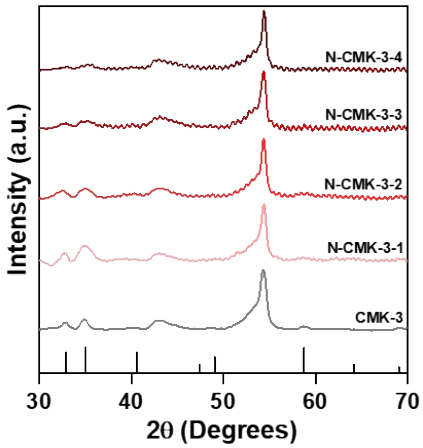

Figure S10. X-ray diffraction (XRD) patterns of the CMK-3 and N-CMK-3 electrodes discharged in 1 M LiTFSI/tetraglyme under dry air. All the XRD data are normalized to the intensity of Carbon+CP peak at 2θ = 54.3. XRD peak positions for standard Li_2O_2 sample are shown by black vertical lines at the bottom

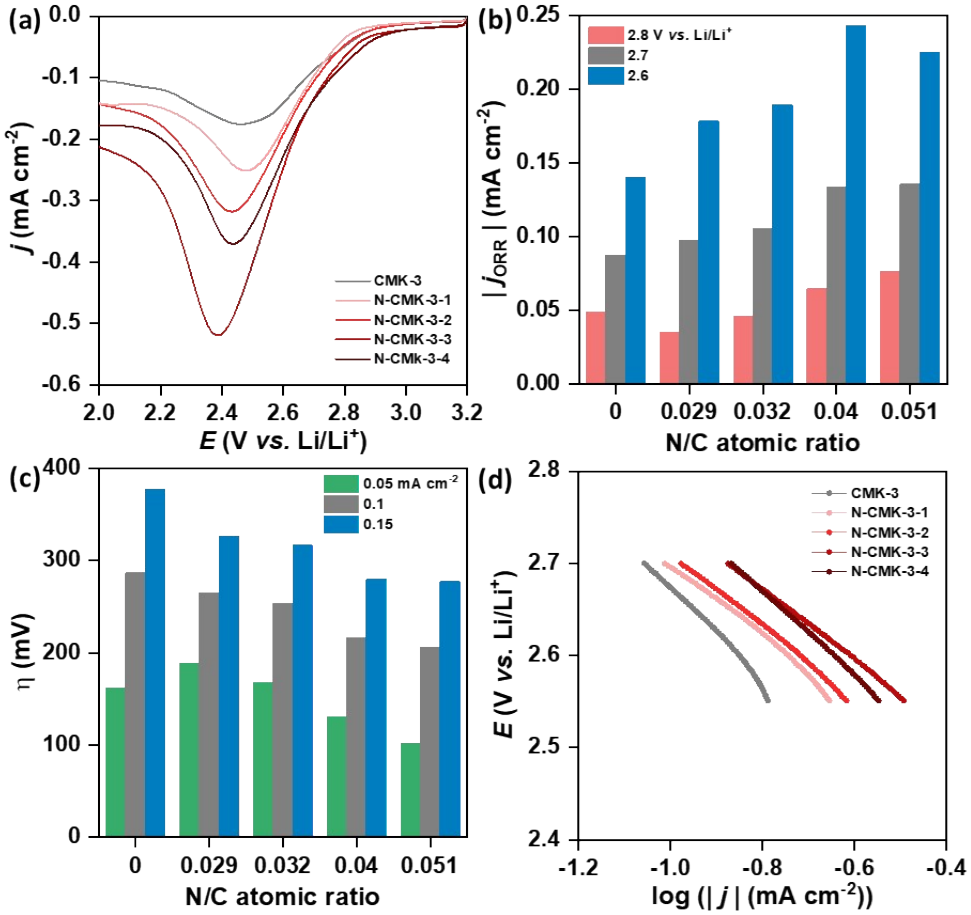

Figure S11. (a) Cathodic linear sweep voltammetry (LSV) of CMK-3 and N-CMK-3 electrodes in the potential range 3.2-2 V *vs*. Li/Li^+ at a sweep rate of 0.5 mV s^{-1} in 1 M LiTFSI/tetraglyme electrolyte, (b) Oxygen reduction current densities for these electrodes at three different potentials, 2.8, 2.7 and 2.6 V *vs*. Li/Li^+, (c) Overpotential required to reach three different ORR current densities, 0.05, 0.1 and 0.15 mA cm^{-2} and (d) Tafel plot in the potential range 2.55 to 2.7 V *vs*. Li/Li^+.

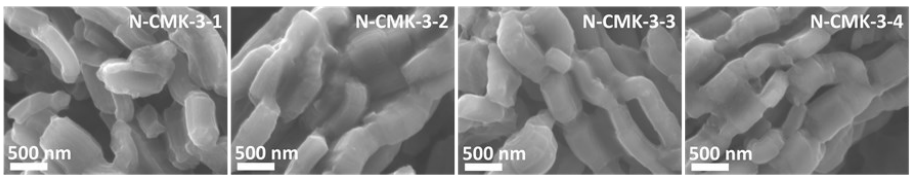

Figure S12. SEM images of N-CMK-3 electrodes after DC in 1 M LiTFSI/tetraglyme electrolyte.

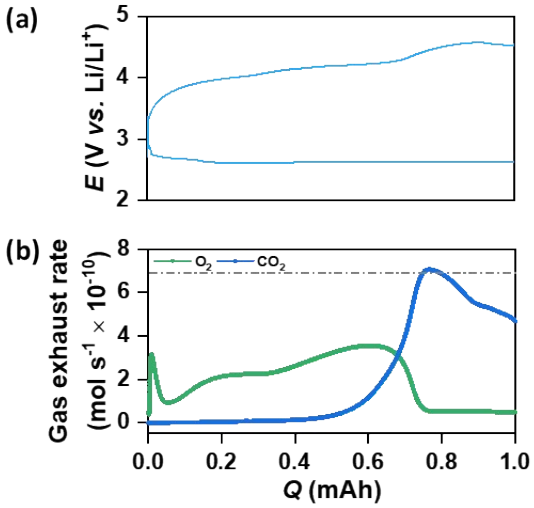

Figure S13. (a) Galvanostatic DC/RC profiles of CNT electrode in 1 M LiTFSI/tetraglyme electrolyte up to a fixed capacity of 1 mAh at 100 mA g^{-1} and (b) corresponding in situ gas evolution data during recharge of the cell.

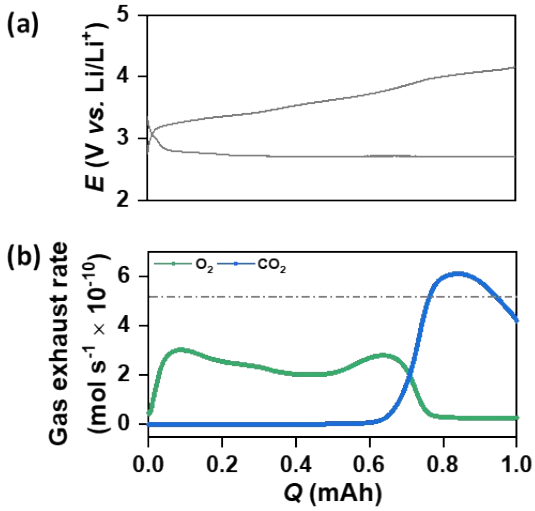

Figure S14. (a) Galvanostatic DC/RC profiles of mesoporous CMK-3 electrode in 1 M LiTFSI/tetraglyme electrolyte up to a fixed capacity of 1 mAh at 100 mA g^{-1} and (b) corresponding in situ gas evolution data during recharge of the cell.

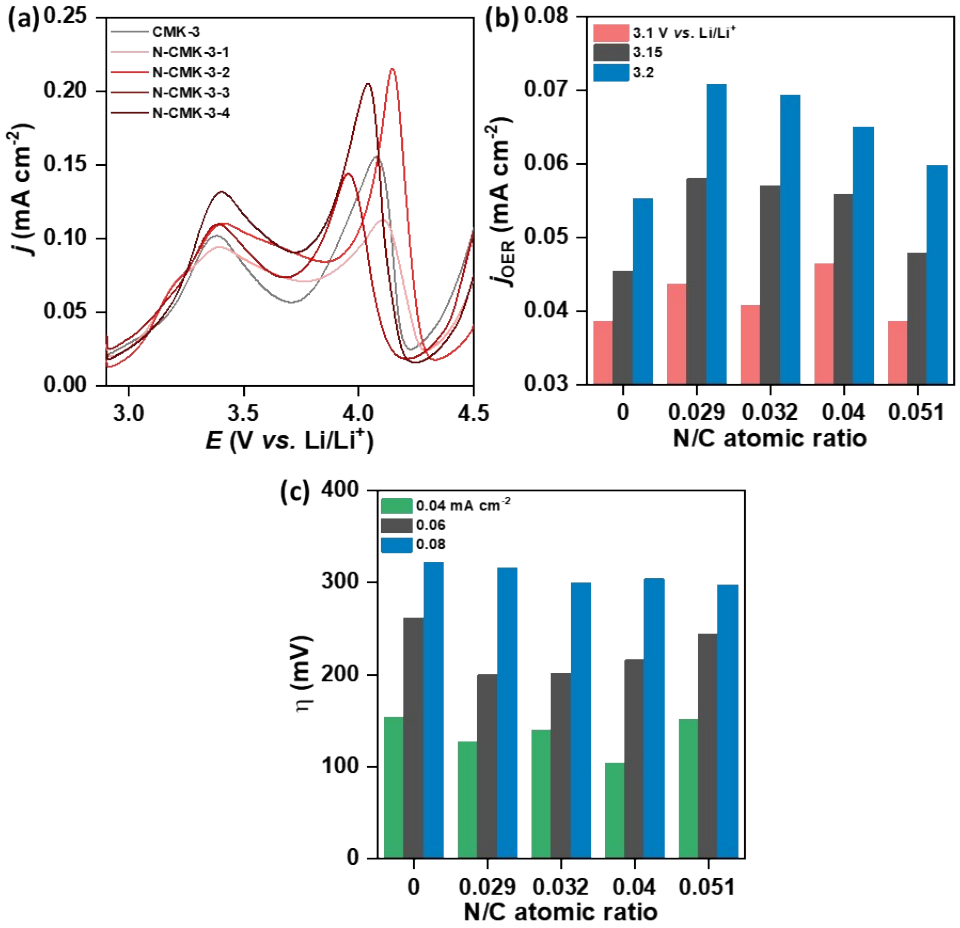

Figure S15. (a) Anodic linear sweep voltammetry (LSV) following a 0.5 mAh cm^{-2} DC of CMK-3 and N-CMK-3 electrodes in the potential range 2.9 to 4.5 V *vs*. Li/Li^+ at a sweep rate of 0.05 mV s^{-1} in 1 M LiTFSI/tetraglyme electrolyte, (b) Oxygen evolution current densities for these electrodes at three different potentials, 3.1, 3.15 and 3.2 V *vs*. Li/Li^+, (c) Overpotential required to reach three different current densities, 0.04, 0.06 and 0.08 mA cm^{-2}.

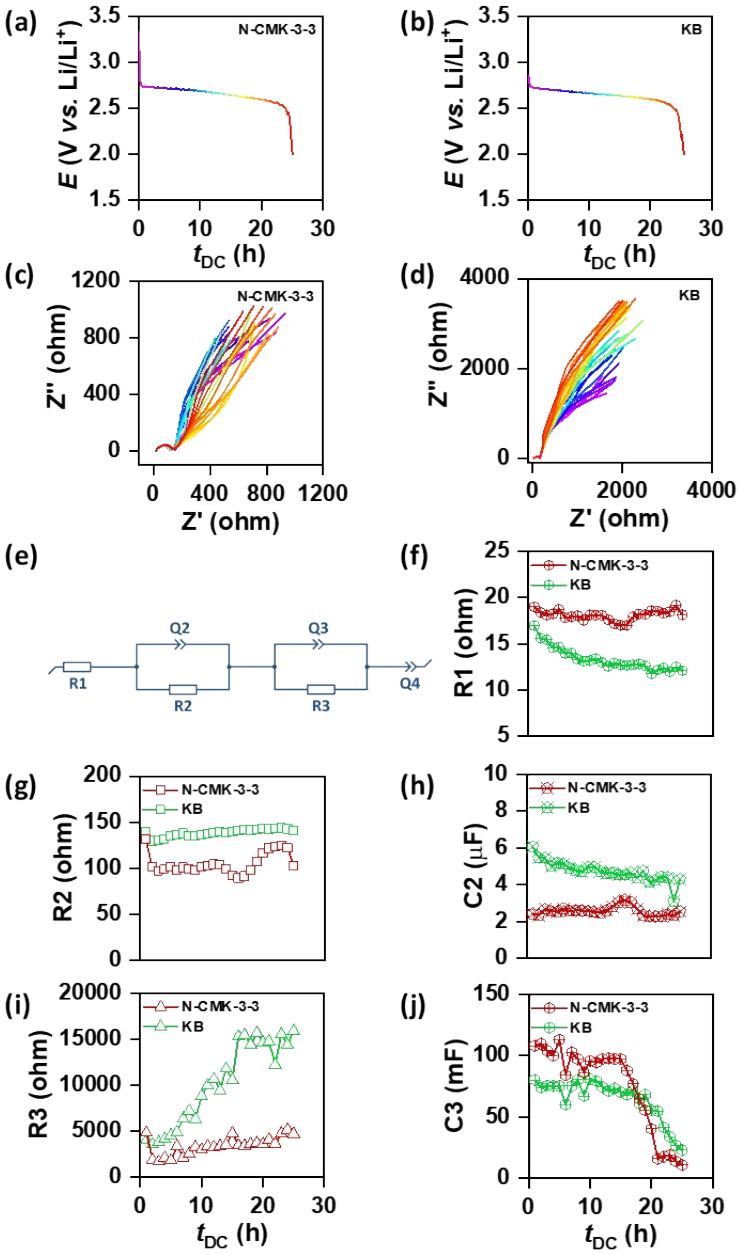

Figure S16. DC curves of (a) N-CMK-3-3 and (b) KB at 100 mA g^{-1} under dry air. Nyquist plots of the cells with (c) N-CMK-3-3 and (d) KB electrodes measured at 1 h interval during DC. The color coding in (c) and (d) corresponds to color coding of DC curves in (a) and (b). (e) shows the equivalent circuit used to fit impedance data in (c) and (d). R1, represented by the intercept on the real Z'-axis at high frequency, corresponds to the ohmic resistance of the cell originating from the resistances of the electrolyte as well of the current collectors. The high frequency R2-Q2 element can be associated with charge transfer processes on the Li surface. The R3-Q3 element has been assigned to processes on the carbon electrode and this is overlapped with a diffusion process represented by Q4 at low frequency. The values of R1 are shown in (f). The values of R2 and the capacitance calculated[5] from Q2 and the same for R3 and Q3 are given in (g, h) and (i, j) respectively. Quite constant values of R2 in the range 120±20 Ω and capacitance in the μF range indicate these processes to be associated with Li metal surface[6]. Much higher values of R3 and capacitance indicate processes in the carbon electrode where increase in R3 values during DC is ascribed to deposition of Li_2O_2. Significantly lower values of R3 for N-CMK-3-3 electrode proves the benefits of nanocrystalline Li_2O_2.

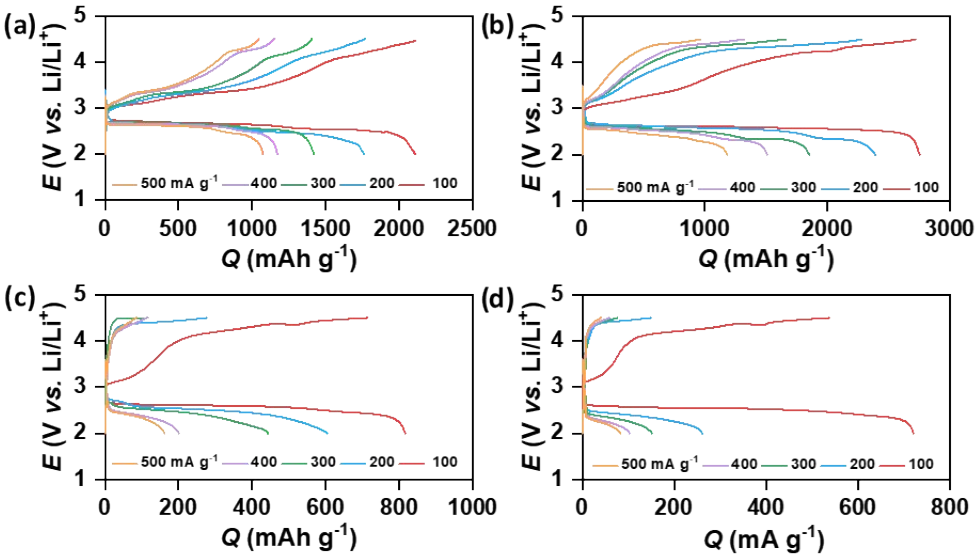

Figure S17. Galvanostatic DC/RC profiles of Li–Air cells with (a) N-CMK-3-3, (b) KB, (c) CNT and (d) SP electrodes in 1 M LiTFSI/tetraglyme electrolyte in the potential range 2–4.5 V *vs*. Li/Li$^+$ at five different current densities in the range 100 to 500 mA g^{-1}.

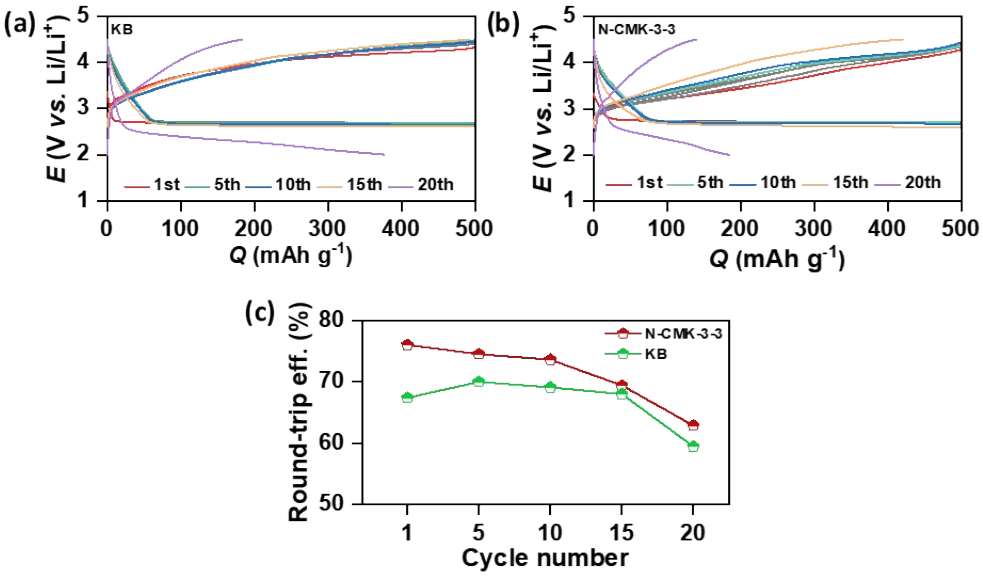

Figure S18. Galvanostatic cycles of (a) KB and (b) N-CMK-3-3 electrodes in 1 M LiTFSI/tetraglyme electrolyte at 100 mA g^{-1}. (c) Comparison of round-trip efficiencies of KB and N-CMK-3-3 electrodes calculated from (a) and (b).

References

1. A. Dutta, R. A. Wong, W. Park, K. Yamanaka, T, Ohta, Y. Jung, H. R. Byon, *Nat. Commun.,* 2018, **9**, 680.
2. A. Dutta, K. Ito, Y. Kubo, *J. Mater. Chem. A,* 2019, **7**, 23199.
3. F. S. Gittleson, R. E. Jones, D. K. Ward, M. E. Foster, *Energy Environ. Sci.,* 2017, **10**, 1167.
4. M. Saito, S. Yamada, T. Ishikawa, H. Otsuka, K. Ito, Y. Kubo, *RSC Adv.,* 2017, **7**, 49031.
5. B. Hirschorna, M. E. Orazema, B. Tribollet, V. Vivierb, I. Frateurc, M. Musianid, *Electrochim. Acta*, 2010, **55**, 6218.
6. J. Højberg, B. D. McCloskey, J. Hjelm, T. Vegge, K. Johansen, P. Norby, A. C. Luntz, *ACS Appl. Mater. Interfaces*, 2015, **7**, 4039.